Supporting Information

Ni@NiO Core/Shell Dendrites for Ultra-Long Cycle Life Electrochemical Energy Storage

Yan Liu,[a] Nianqing Fu,[a] Guoge Zhang,[b] Wei Lu,[a] Limin Zhou,[c] and Haitao Huang[a]*

[a] Department of Applied Physics and Materials Research Center, The Hong Kong Polytechnic University, Hung Hom, Kowloon, Hong Kong, China.

E-mail address: aphhuang@polyu.edu.hk

[b] School of Materials Science and Engineering, South China University of Technology, Guangzhou, 510640, P. R. China

[c] Department of Mechanical Engineering, The Hong Kong Polytechnic University, Hung Hom, Kowloon, Hong Kong, China

Contents

Section A. Calculations

Specific capacitance: The specific capacitance (*C*) of the electrode was calculated from the CV curves,

$$C = \frac{\int I(V)dV}{2v \times V \times S} \quad \text{(S1)}$$

where *I*(*V*) is the response current density (A), *v* is the scan rate (V/s), *V* is the potential window (V), and *S* is the active weight or area of the electrode (g or cm^2). The mass density of the as-prepared electrode was 0.7 mg cm^{-2}. The mass of the active materials was calculated as the mass difference between the nickel substrate before and after the electrodeposition.

The capacitance can also be calculated from the discharging curves,

$$C = \frac{I \times \Delta t}{\Delta V \times S} \quad \text{(S2)}$$

where *I* is the charge/discharge current (A), *Δt* is the time for a full discharge (s), *ΔV* is the potential window during a full charge/discharge (V), and *S* is the weight of the active material or the apparent area of the electrode (g or cm^2).

Section B. Supplementary figures (Figure S1-S18)

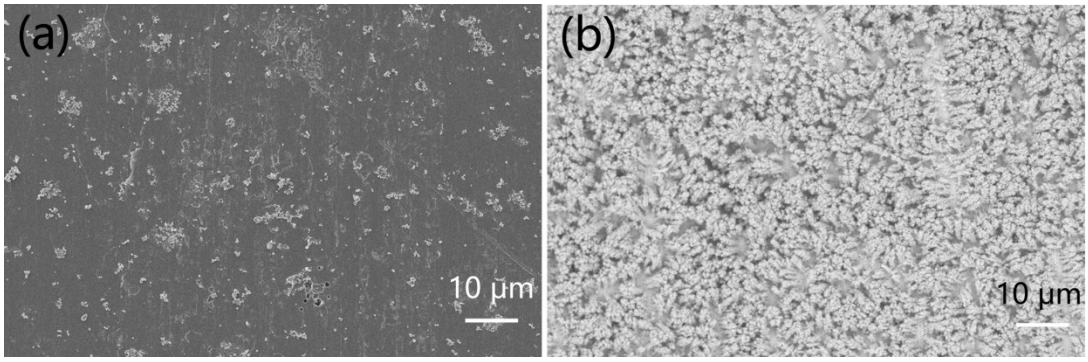

Figure S1. Surface morphologies of (a) anode and (b) cathode after electrodeposition in EG electrolyte at 40°C.

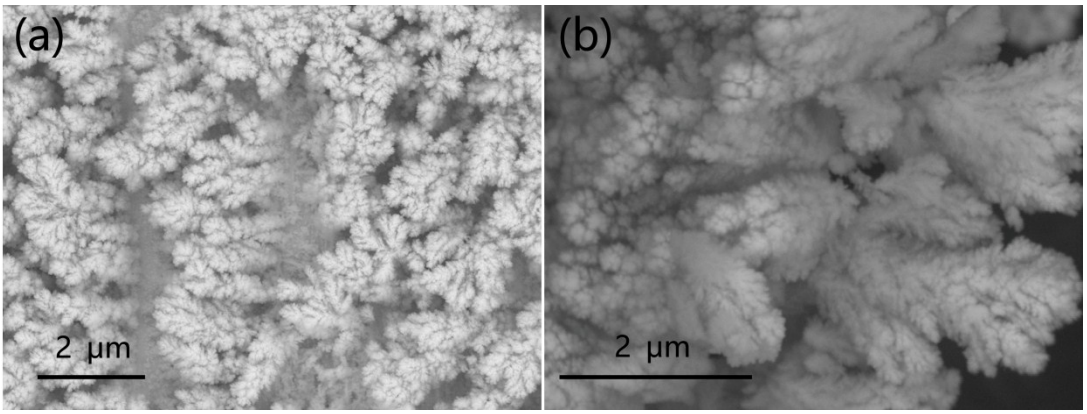

Figure S2. SEM image with (a) top view and (b) cross-sectional view of the microstructure of DNE material.

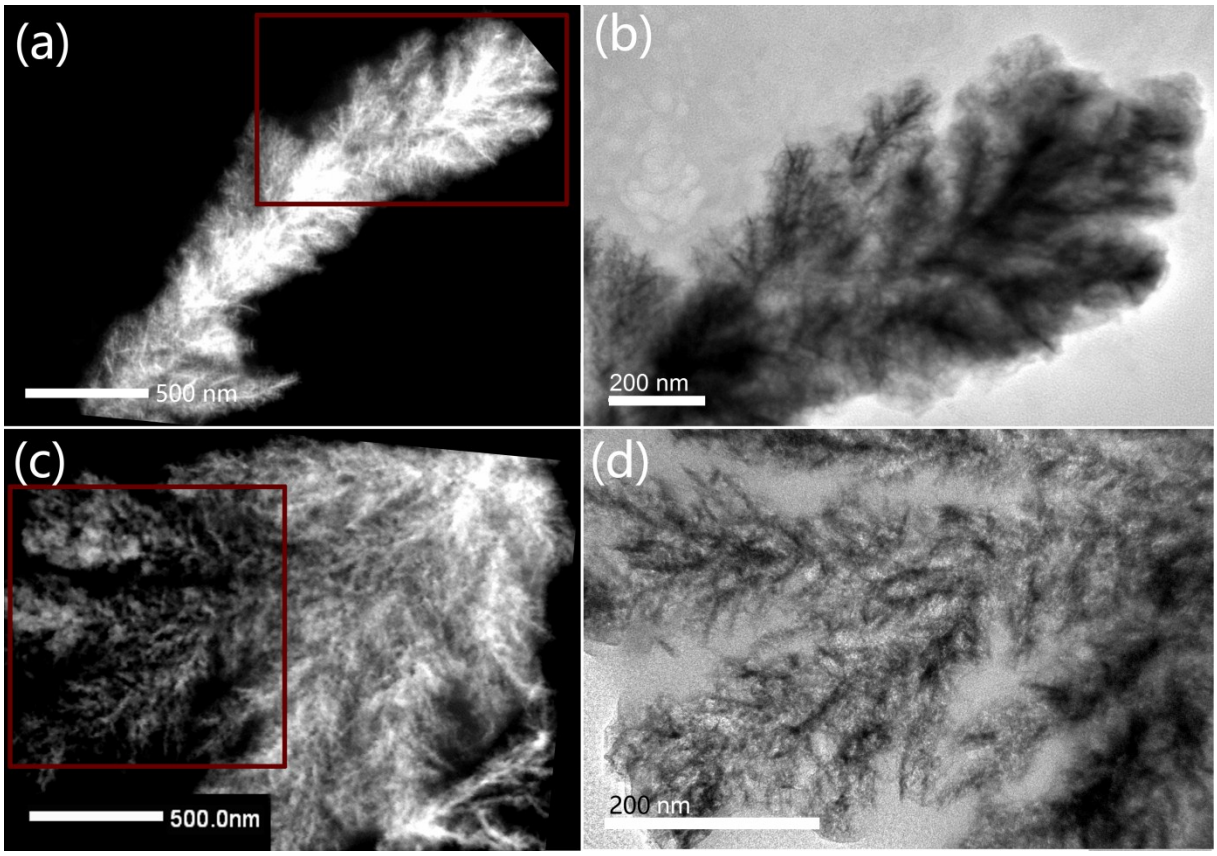

Figure S3. TEM characterization of DNE materials in different selected areas of the same sample.

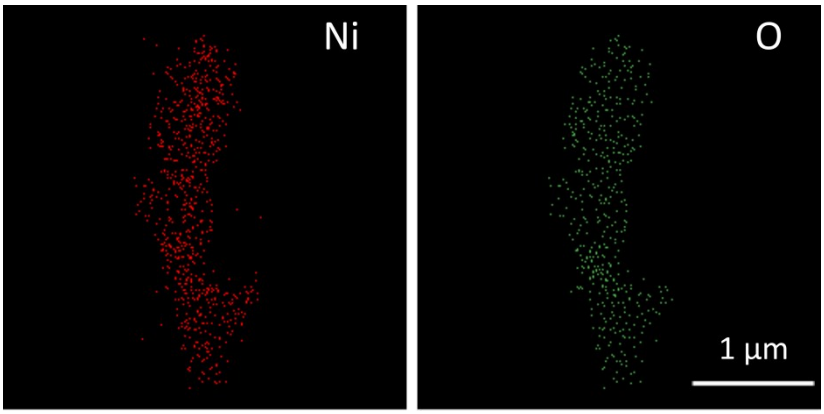

Figure S4. The element mapping of DNE materials.

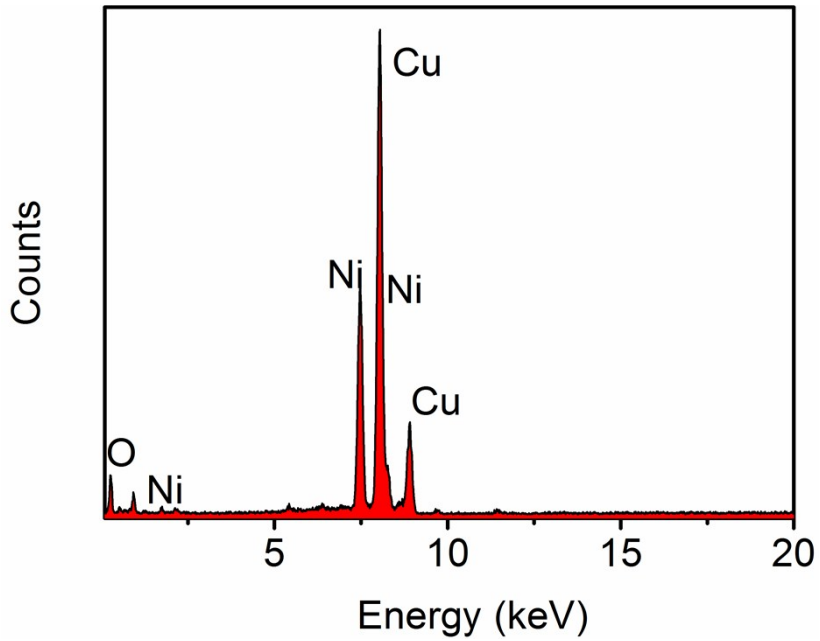

Figure S5. The corresponding EDS of the marked area of Figure 1(d). The Cu signal comes from the TEM sample holder.

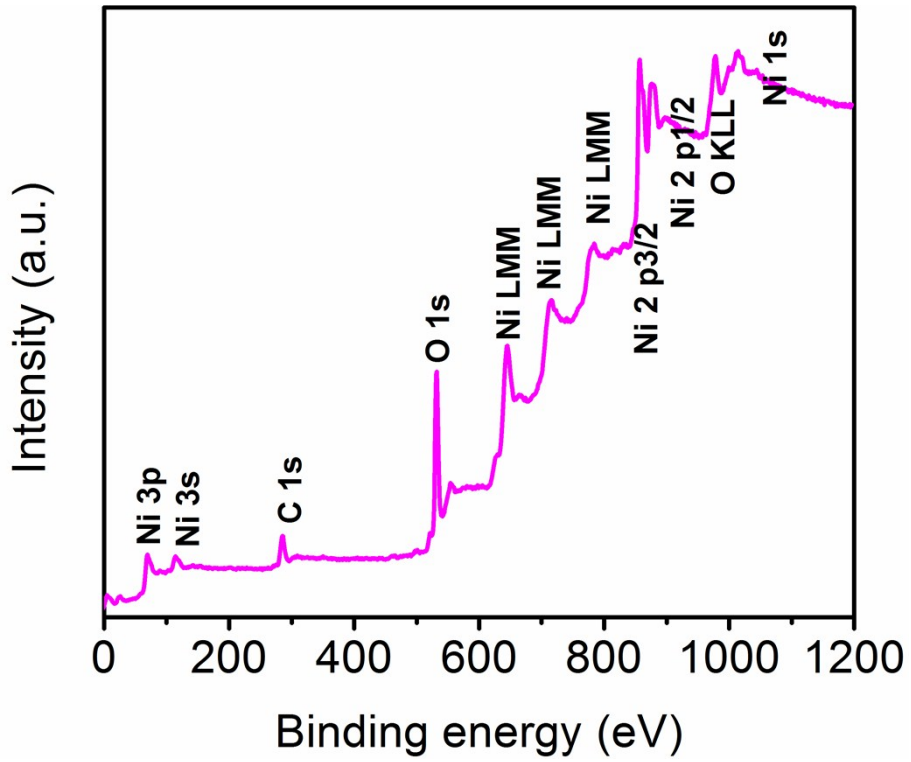

Figure S6. Full XPS pattern of the DNE material.

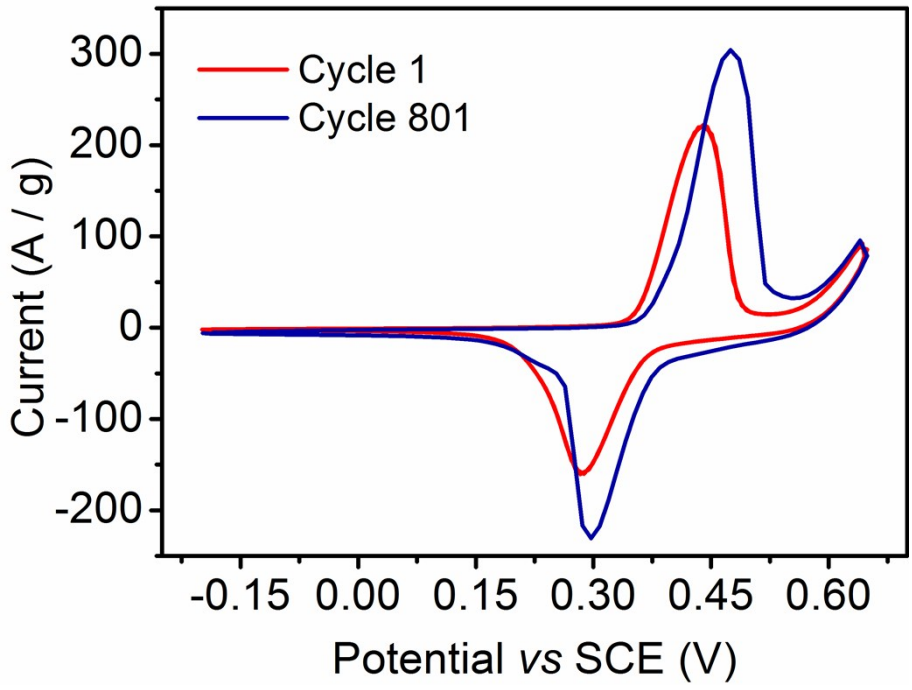

Figure S7. CV curves of the 1st and the 801st cycles at a scan rate of 100 mV s^{-1}.

Table S1. Comparison of the maximum specific capacitance of some reported nickel-based electrode and the present work.

Electrode materials	Mass loading (mg/cm^2)	Electrolyte	Current density ($A\ g^{-1}$)	Specific capacitance ($F\ g^{-1}$)	Ref.
Ni/NiO	0.7	1 M NaOH	2.9	1928.5	Present work
$Ni(OH)_2/NiF_2$	0.15	1 M NaOH	2	350.0	1
Ni-Co LDH	0.23±0.02	6 M KOH	1	1760.0	2
NiO/Co_3O_4	N/A	1 M KOH	4	1190.0	3
Ni-CNTs@β-$Ni(OH)_2$	N/A	1 M KOH	2	1807.0	4
Ni/NiO NTs	N/A	1 M NaOH	1	<1000	5
rGO/a-$Ni(OH)_2$	0.8	1 M KOH	1	1671.1	6

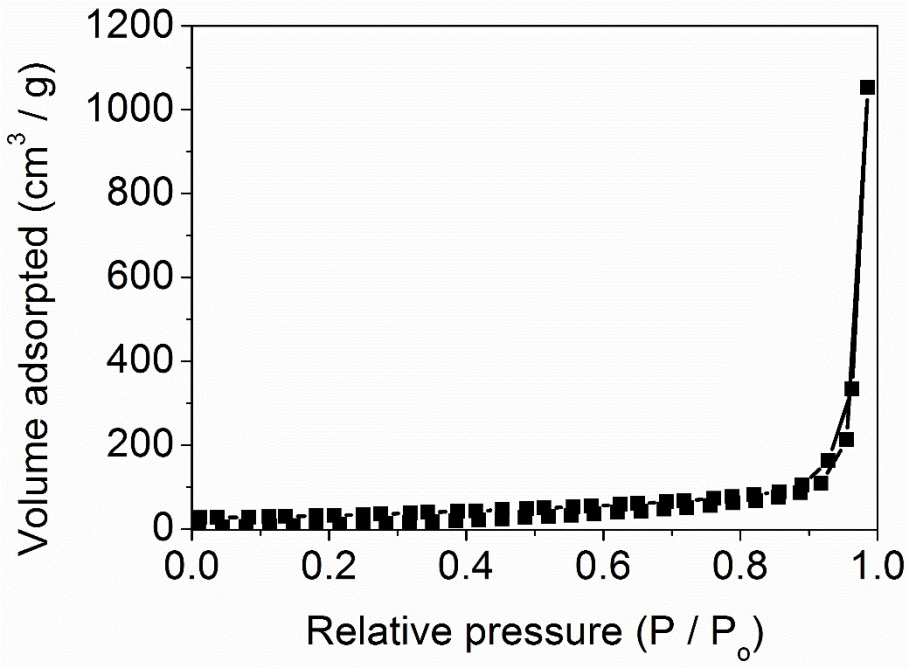

Figure S8. BET isothermal of DNE material.

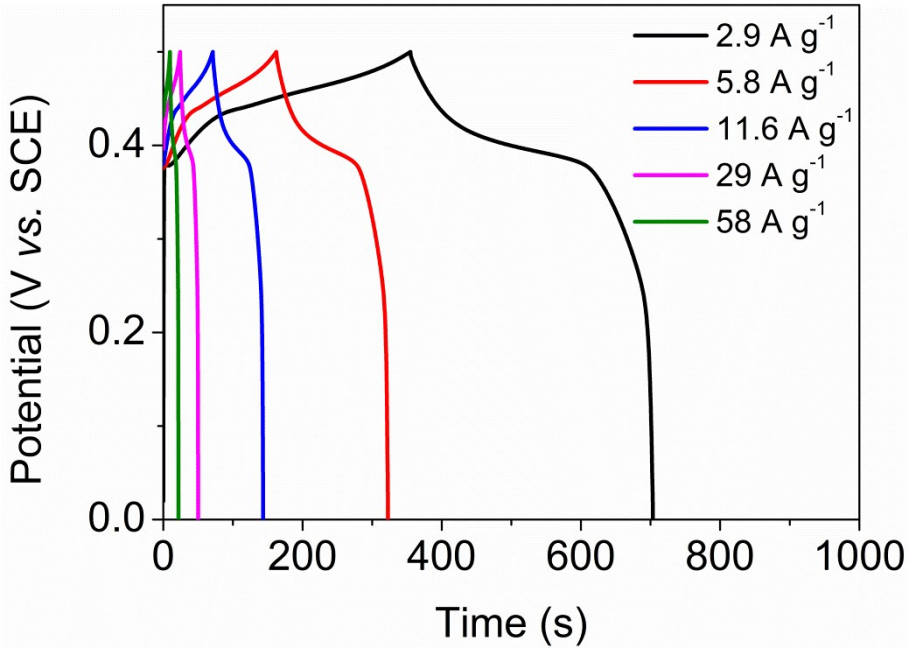

Figure S9. GCD of the DNE at the different current densities.

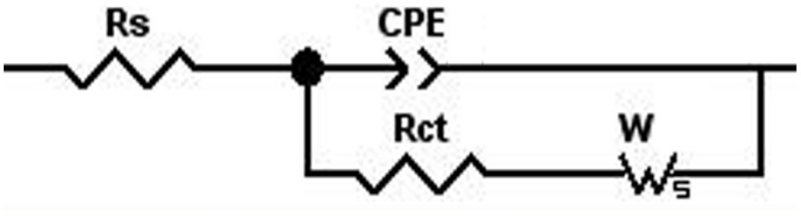

Figure S10. Equivalent circuit of the DNE. R_s is the equivalent internal resistance, including resistance of the electrolyte and the internal resistance of the electrode. *W* is the finite-length Warburg diffusion element, R_{ct} is charge transfer resistance, and CPE is the constant phase element [7].

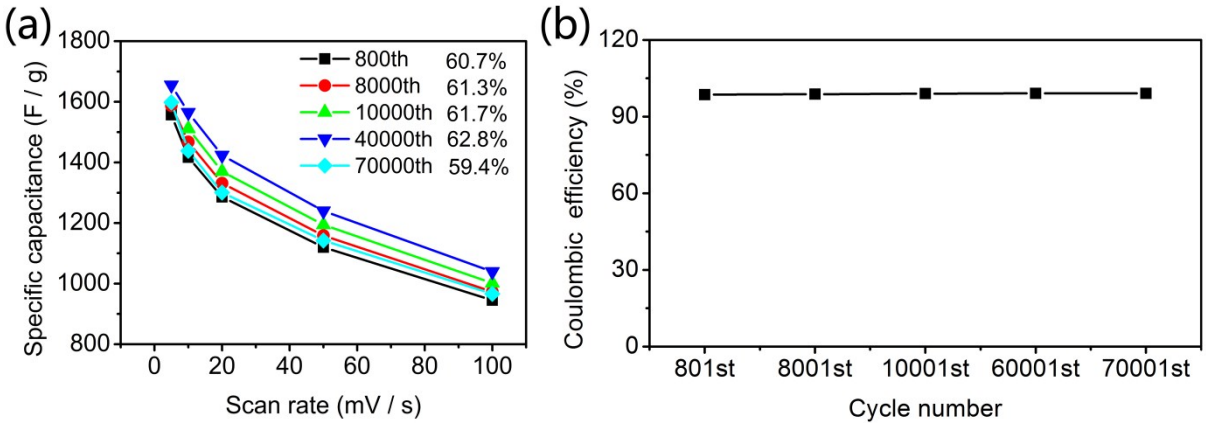

Figure S11. (a) Specific capacitance as a function of scan rate and (b) Coulombic efficiency at different cycling stages.

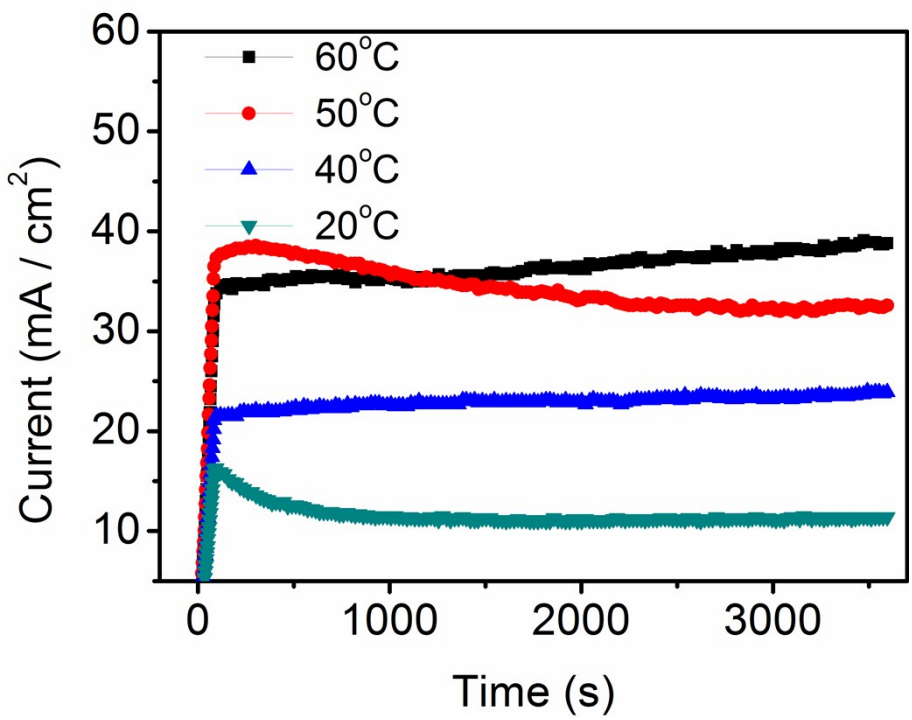

Figure S12. The current transient of the electrodeposition process at different temperatures.

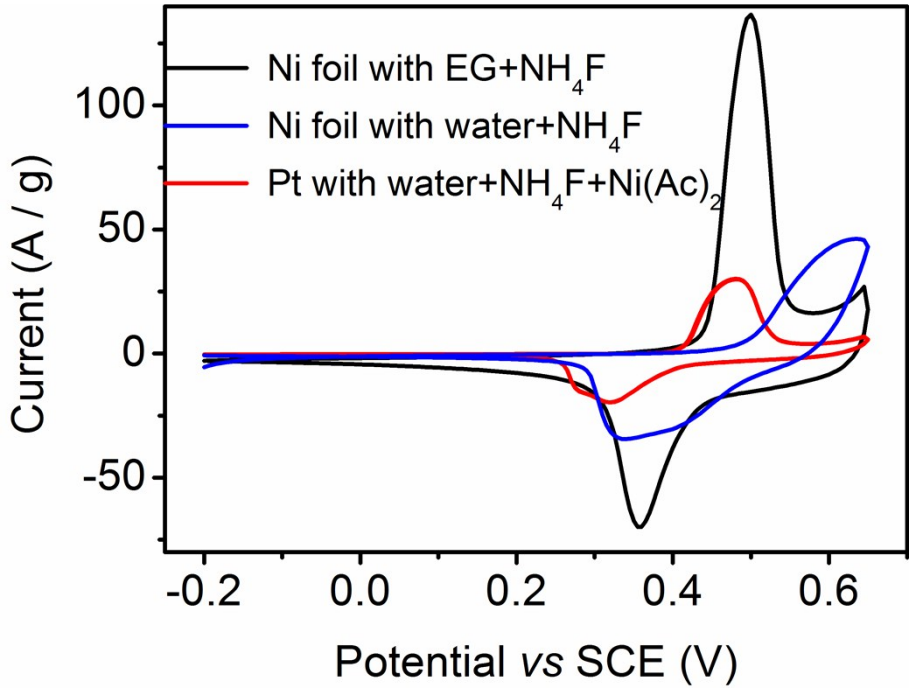

Figure S13. CV curves of samples in different electrolytes at a scan rate of 20 mV s^{-1}.

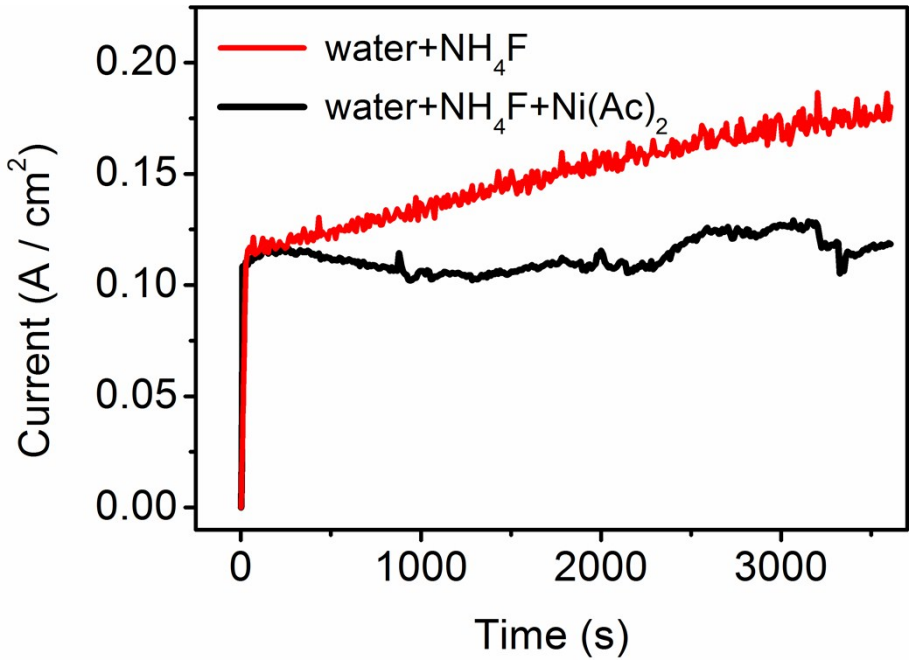

Figure S14. The current transient of the electrodeposition process in different electrolytes.

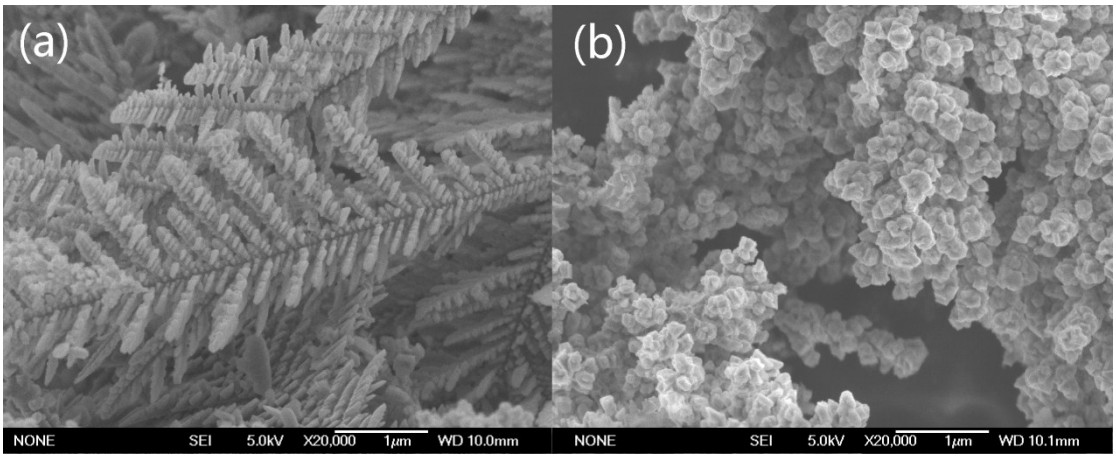

Figure S15. SEM images of samples prepared in different electrolytes containing (a) water+NH_4F in which the nickel anode was the nickel source and (b) water+ NH_4F +0.05 mol L^{-1} $Ni(Ac)_2$ where platinum was used as the anode.

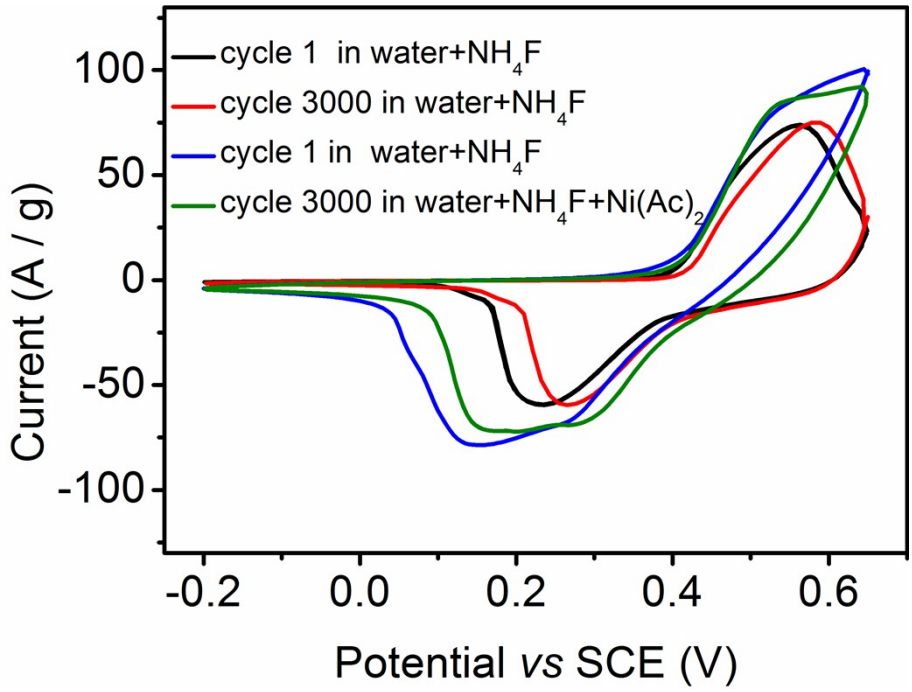

Figure S16. Cyclic test of samples prepared in different electrolytes containing (1) water+0.1% NH_4F in which nickel anode was the nickel source and (2) water+ 0.1% NH_4F +0.05 mol L^{-1} $Ni(Ac)_2$ where platinum was used as the anode, at a scan rate of 100 mV s^{-1}.

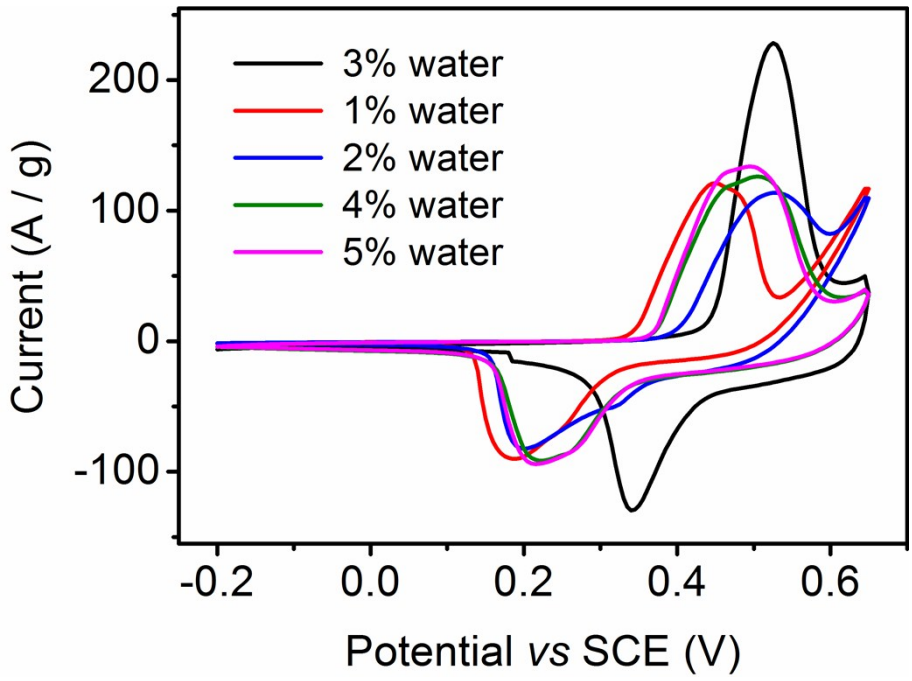

Figure S17. The CV curves of samples prepared in EG electrolyte containing 0.1% NH_4F with different water contents at a scan rate of 100 mV s^{-1}.

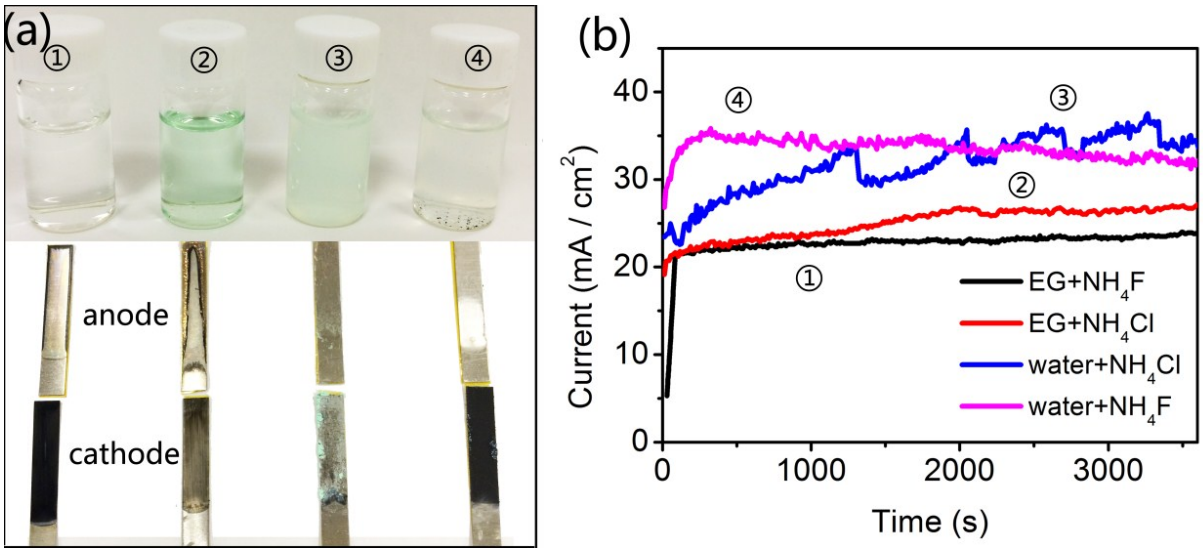

Figure S18. (a) Digital pictures of samples prepared at 40°C in different electrolytes, EG+NH_4F (①), EG+NH_4Cl (②), water+NH_4Cl (③), and water+NH_4F (④). Inside the bottles are the electrolyte solutions after electrodeposition reaction. (b) The current transient of the electrodeposition process in electrolytes at 40°C. The applied voltages are 60, 30, 7, and 7 V, respectively.

In order to further understand that electrolyte plays an important role in the electrodeposition reaction, even if nickel foil is still used as the anode, Figure S18a exhibits the samples which were prepared in different electrolytes where NH_4Cl was instead of NH_4F and DI water was instead of EG. Sample ① was prepared by our work. The DNE material was uniformly grown on the surface of nickel foil. From Equation S3-S5 [8-10], fluorine ions could prevent the fast dissolution of nickel by the formation of NiF_4^{2-} on the surface of the nickel. So, the electrolyte after the reaction was clear (Figure S18a①) and current response value kept unchanged (Figure S18b①). The results demonstrate that a stable nickel source is good for the formation of a stable coating layer. When NH_4Cl took place of NH_4F, the dissolution of nickel of sample ② as the anode was faster than that of sample ① which can be surmised from the larger current density (Figure S18②). Moreover, the colour of the

electrolyte (Figure S18b②) was dark green belonging to nickel ions; the anode was seriously corroded; chloride ions can also strengthen the corrosion level. Amount of H_2 obstructs the adhesion of active materials on the cathode; therefore, it is difficult to form a coating layer. The experimental results of sample ① and ② express the role of NH_4F in the preparation of the DNE material. While EG was replaced by DI water and NH_4Cl was instead of NH_4F, it is impossible to form a coating layer (Figure S18a③). Almost all the active materials were flaked off into the electrolyte solution which exhibited the cloudiness state. The current response (Figure S18b③) was unstable and ratcheted upward, indicating the circulation between adhesion and flaking of the active materials on the cathode. If only EG was replaced by DI water, the coating layer of sample ④ was better than those of sample ② and ③. However, it was observed that the black materials fell in the electrolyte solution, and there were two kinds of materials with different colours on the surface of the cathode (Figure S18a④). What's more, the current response was stable (Figure S18b④). The results of sample ③ and ④ indicate that the fast ion diffusion in DI water due to its low viscosity harms the formation of the coating layer where active ions have no time to react or the products were washed off due to much H_2 that originates from hydrogen evolution on the cathode.

$$Ni^{2+} + 2F^- \rightarrow NiF_2 \quad (S3)$$

$$NiF_2 + 2F^- \rightarrow NiF_4^{2-} \quad (S4)$$

$$NiO + 4F^- + 2H^+ \rightarrow NiF_4^{2-} + H_2O \quad (S5)$$

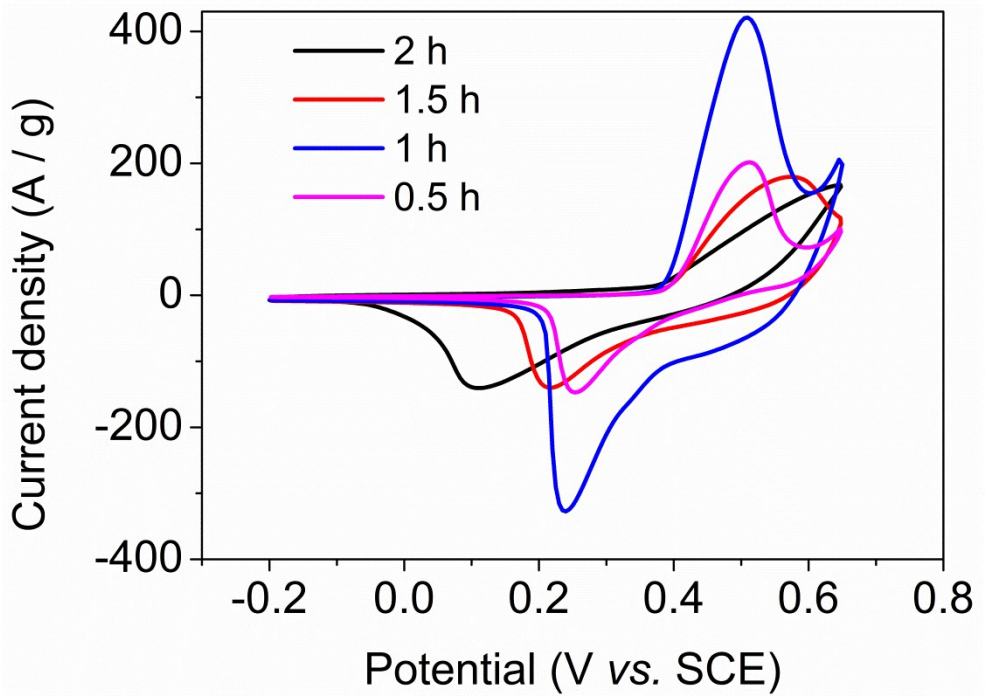

Figure S19. The CV curves of samples prepared with different deposition time duration.

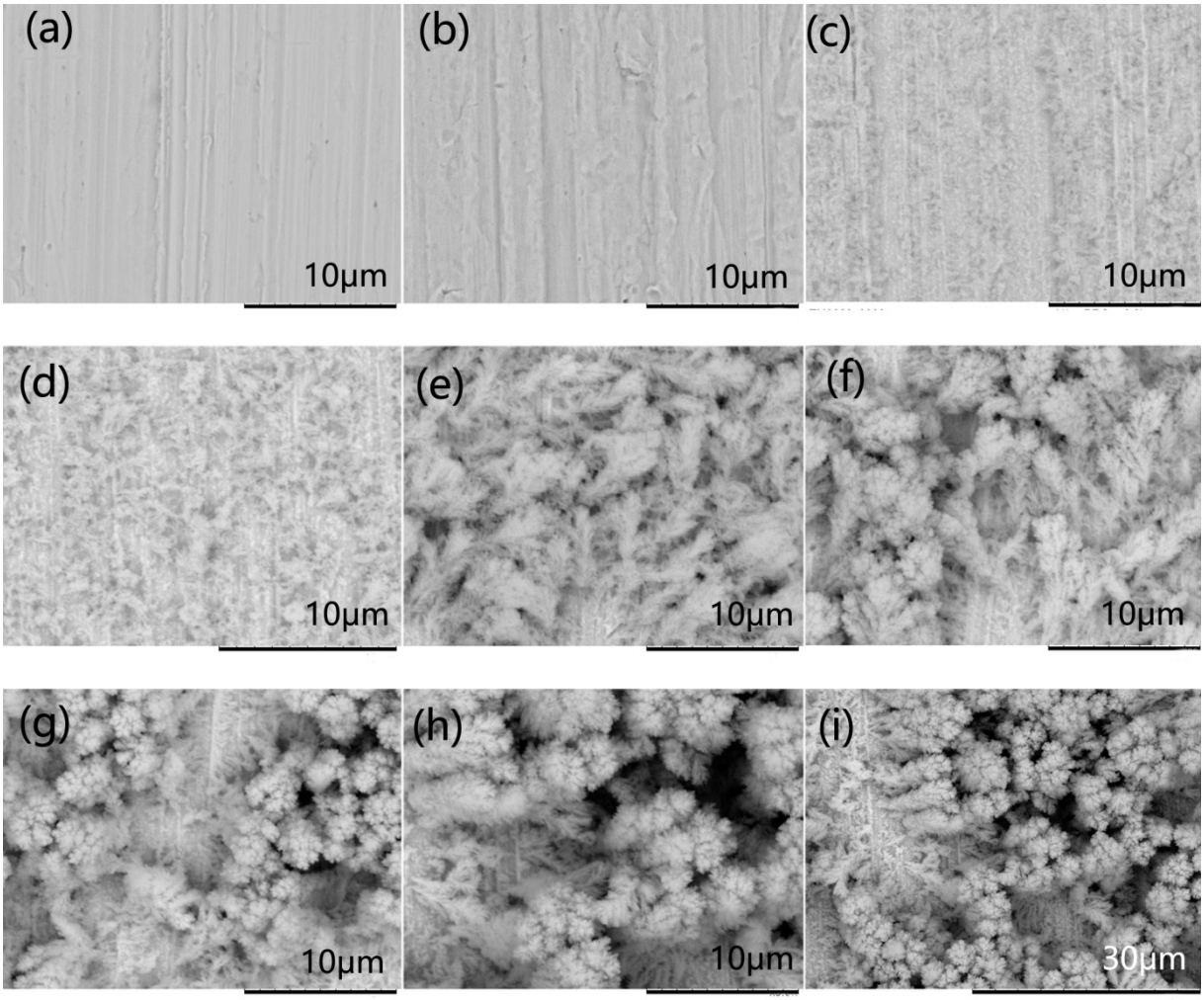

Figure S20. The morphology evolution of cathode surface at 40°C after electrodeposition of (a) 0, (b) 0.5, (c) 2, (d) 5, (e) 10, (f) 20, (g) 30, and (h, i) 60 min.

Section C. Supporting references

1. M. Jin, G. Zhang, F. Yu, W. Li, W. Lu and H. Huang, *Phys. Chem. Chem. Phys.*, 2013, **15**, 1601-1605.
2. M. Yang, H. Cheng, Y. Gu, Z. Sun, J. Hu, L. Cao, F. Lv, M. Li, W. Wang, Z. Wang, S. Wu, H. Liu and Z. Lu, *Nano Res.*, 2015, **8**, 2744-2754.
3. K. Xu, R. Zou, W. Li, Y. Xue, G. Song, Q. Liu, X. Liu and J. Hu, *J. Mater. Chem. A*, 2013, **1**, 9107-9113.

4. X. Ma, Y. Li, Z. Wen, F. Gao, C. Liang and R. Che, *ACS Appl. Mater. Interfaces*, 2015, **7**, 974-979.
5. Q. Li, C.-L. Liang, X.-F. Lu, Y.-X. Tong and G.-R. Li, *J. Mater. Chem. A*, 2015, **3**, 6432-6439.
6. S. Bag and C. R. Raj, *J. Mater. Chem. A*, 2014, **2**, 17848-17856.
7. L. Wang, X. Feng, L. T. Ren, Q. H. Piao, J. Q. Zhong, Y. B. Wang, H. W. Li, Y. F. Chen and B. Wang, *J. Am. Chem. Soc.*, 2015, **137**, 4920-4923.
8. B. A. Lange and H. M. Haendler, *J. Inorg. Nucl. Chem.*, 1973, **35**, 3129-3133.
9. I. Sheft, H. H. Hyman and J. J. Katz, *J. Am. Chem. Soc.*, 1953, **75**, 5221-5223.
10. N. K. Allam and C. A. Grimes, *J. Phys. Chem. C.*, 2007, **111**, 13028-13032.